Scientia Iranica C (2015) 22(6), 2298–2308

Sharif University of Technology
Scientia Iranica
Transactions C: Chemistry and Chemical Engineering
www.scientiairanica.com

Crystal structure, spectroscopic characterization, and computational study of two new 4-aminobenzoic acid derived Schiff base ligands

R. Kia[a,*] and H. Kargar[b]

a. *Department of Chemistry, Sharif University of Technology, Tehran, P.O. Box 11155-3516, Iran.*
b. *Department of Chemistry, Payame Noor University, Tehran, P.O. Box 19395-3697, Iran.*

Received 6 September 2014; received in revised form 15 February 2015; accepted 1 August 2015

KEYWORDS
Schiff base ligands;
Diimine ligands;
N,O-donor ligands;
X-ray diffraction;
Density Functional Theory (DFT).

Abstract. Two new Schiff base ligands, (*E*)-4-(3-ethoxy-2-hydroxybenzylideneamino) benzoic acid ($\mathbf{L}^1$) and (*E*)-4-(3-methoxy-2-hydroxy-benzylideneamino)benzoic acid ($\mathbf{L}^2$), were synthesized and characterized by elemental analyses, FT-IR, NMR spectroscopy and single-crystal X-ray diffraction analysis. The compound, $\mathbf{L}^1$, was crystallized in the triclinic system, space group $P-1$, with $a = 4.9897(3)$ Å, $b = 6.9109(5)$ Å, $c = 20.7694(15)$ Å, $\alpha = 83.690(4)^\circ$, $\beta = 84.855(4)^\circ$, $\gamma = 78.698(4)^\circ$, $V = 696.35(8)$ Å^3, and $Z = 2$. The compound $\mathbf{L}^2$ was crystallized in the orthorhombic system, non-centerosymmetric space group, $P2_12_12_1$, with $a = 4.7824(4)$ Å, $b = 10.2031(11)$ Å, $c = 30.516(3)$ Å, $V = 1489.0(3)$ Å^3, and $Z = 4$. Both $\mathbf{L}^1$ and $\mathbf{L}^2$ display a trans-configuration about the C=N double bond. The Density Functional Theory (DFT) and the Time-Dependent Density Functional Theory (TD-DFT) were used to study the ground state properties (molecular orbitals), and interpret the absorption spectra of these ligands, respectively. Electronic Difference Density Maps (EDDMs) were calculated from the TD-DFT study, indicating the change of electron density in the singlet excited states.

1. Introduction

Schiff bases are among the most prevalent mixed donor ligands in the field of coordination chemistry, which are normally formed by the condensation reaction of a primary amine and a carbonyl group. Depending on the starting carbonyl compound, they are named as aldimine or ketimine for aldehyde or ketone, respectively [1]. They show a variety of biological activity, including antibacterial, antifungal, anticancer, and herbicidal activities [2,3]. In the field of coordination chemistry, they are capable of forming complexes with different transition and lanthanide metal ions, showing pharmacological properties, i.e. toxicity against bacterial/fungal growth, and anticancer and antitumor activity [4-6]. Furthermore, they are also important compounds in dye and plastic industries, as well as in the field of liquid crystal technology [7,8]. Schiff base ligands, derived from salicylaldehyde or substituted-salicylaldehyde and mono-amino carboxylic acids, belong to a family of coordinating ligands having potential coordination sites for donation involving O-phenolic, N-iminic and carboxylate oxygen atoms, which are potentially bidentate donor ligands. They have also attracted considerable attention because of their application in photochromic lenses [9], rewritable papers [10], photo-switching materials [11], and optical data storage materials [12]. Among different Schiff base ligands, salicylideneaniline (SA) derivatives are well known as photochromic compounds, undergoing

*. *Corresponding author. Tel.: +98 21 66165332*
E-mail addresses: rkia@sharif.edu & zsrkk@yahoo.com (R. Kia); h.kargar@pnu.ac.ir (H. Kargar)

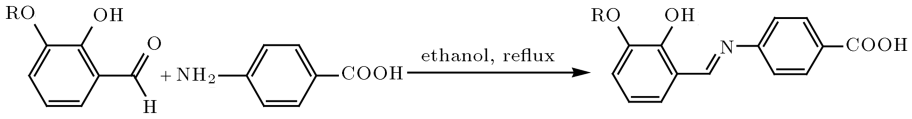

L¹, R=-CH_2CH_3
L², R=-CH_3

Scheme 1. Preparation route for the ligands.

a color change from yellow to red upon irradiation with UV light, and the reverse color change upon exposure to visible light or heat, which is due to the tautomerization between phenol-imine and keto-amine forms [13]. Systematic studies in the structure-properties relationship of SA derivatives have shown that crystals with a non-planar molecular conformation exhibit photochromic properties, and those with a planar molecular conformation are non-photochromic and exhibit thermochromic properties [14]. Another important application of carboxylated Schiff base ligands, based on their Cu(I) and Ru(II) complexes, is in preparation of Dye-Sensitized Solar Cells (DSSCs) by anchoring on the surface of TiO_2 nanoparticles for so-called light harvesting applications in the conversion of light to electricity [15-20]. Regarding these various applications, herein, we report the synthesis, spectroscopic characterization, computational studies, and the crystal structure of two new 4-aminobenzoic acid derived Schiff base ligands (Scheme 1).

2. Experimental

2.1. Materials and methods

All chemicals were of reagent grade and used without further purification. Elemental analyses (C, H, and N) were performed on a Leco CHNS-analyzer. ^{1}H NMR and ^{13}C NMR spectra of ligands (*E*)-4-(3-ethoxy-2-hydroxybenzylideneamino)benzoic acid (**L**^{1}) and (*E*)-4-(3-methoxy-2-hydroxybenzylideneamino)benzoic acid (**L**^{2}) were recorded on a BRUKER AVANCE 400 MHz spectrophotometer using DMSO-d^6 as solvent. IR spectra were recorded on an IR Prestige-21 Shimadzu instrument as KBr pellets. The electronic spectra of the ligands were recorded in chloroform on a Cary 5A spectrophotometer.

2.2. Synthesis of L^1 and L^2

L^1: 2-hydroxy-3-ethoxybenzaldehyde (3.32 g, 20 mmol) was added to an ethanolic solution (50 mL) of 4-aminobenzoic acid (2.75 g, 20 mmol) and the mixture was refluxed for 1 h. The yellow precipitates of **L**^{1} were collected by filtration, washed with ethanol and then dried in *vacuo* at room temperature. Yield 2.25 g ($\sim$ 40%). *Anal.* Calc. for $C_{16}H_{15}NO_4$: C, 67.36; H, 5.30; N, 4.91. Found: C, 67.29; H, 5.33; N, 4.87%. IR (KBr, cm^{-1}): ν_{asym} (COO$^-$) 1678, ν_{sym} (COO$^-$) 1423, ν (C=N) 1591, ν (C-N) 1249. ^{1}H NMR (DMSO-*d*6): δ (ppm) 12.87 (br, 1H, H^q), 12.82 (br, 1H, H^p), 8.91 (s, 1H, H^i), 7.94 [d (8 Hz), 1H, H^e], 7.41 [d (8 Hz) 1H, H^d], 7.18 [d (8 Hz), 1H, H^c], 7.05 [d (8 Hz), 1H, H^a], 6.82 [t (8 Hz), 1H, H^b], 3.99 [q (7 Hz), 2H, H^o], 1.27 [t (7 Hz), 3H, H^m]. ^{13}C {^{1}H} NMR (DMSO-d^6): δ (ppm) 166.8, 165.1, 151.8, 150.8, 147.0, 130.7, 128.8, 124.1, 121.5, 119.2, 118.8, 117.2, 64.1, 14.7.

L^2: This ligand was prepared using the same method as **L**^{1}, except that 2-hydroxy-3-methoxybenzaldehyde (3.05 g, 20 mmol) were used. The red precipitates of **L**^{2} were collected by filtration, washed with ethanol and then dried in *vacuo* at room temperature. Yield 2.48 g ($\sim$ 46%). *Anal.* Calc. for $C_{15}H_{13}NO_4$: C, 66.41; H, 4.83; N, 5.16. Found: C, 66.39; H, 4.85; N, 5.12%. IR (KBr, cm^{-1}): ν_{asym} (COO$^-$) 1683, ν_{sym} (COO$^-$) 1425, ν (C=N) 1593, ν (C-N) 1253. ^{1}H NMR (DMSO-*d*6): δ (ppm) 12.87 (br, 1H, H^q), 12.75 (br, 1H, H^p), 8.90 (s, 1H, H^i), 7.93 [d (8 Hz), 1H, H^e], 7.40 [d (8 Hz) 1H, H^d], 7.19 [d (8 Hz), 1H, H^c], 7.07 [d (8 Hz), 1H, H^a], 6.84 [t (8 Hz), 1H, H^b], 3.74 (s, 3H, H^o). ^{13}C{^{1}H}-NMR (DMSO-d^6): δ (ppm) 166.8, 164.9, 151.9, 150.5, 147.9, 130.7, 128.8, 123.8, 121.5, 119.2, 118.8, 115.8, 55.8.

2.3. Crystal structure analysis

The crystals suitable for X-ray crystallography were grown by slow evaporation of ethanol of the ethanolic solutions of **L**^{1} and **L**^{2}. Single crystal X-ray data for **L**^{1} and **L**^{2} were collected at 296(2) K on a Bruker SMART APEXII CCD area detector diffractometer with Mo Kα radiation (λ = 0.71073 Å). Cell parameters were retrieved using SMART [21] software and refined using SAINT [22] on all observed reflections. Data reduction and correction for Lp and decay were performed using SAINT Plus software. Absorption corrections were applied using SADABS [23]. The structure was solved by direct methods and refined by the least squares method on F^2 using the SHELXTL program package [24]. All non-hydrogen atoms were refined anisotropically. Hydrogen atoms were positioned geometrically and refined with a riding model approximation, with their parameters constrained to the parent atom, with U_{iso} (H) = 1.2 or 1.5 U_{eq} (C) and U_{iso} (H) = 1.5 U_{eq} (O) for hydroxyl and carboxylic hydrogen atoms.

2.4. Computational details

For the ground state electronic structure calculations the DFT method, with the Becke [25] three param-

eter hybrid functional and Lee-Yang-Parr's [26] gradient corrected correlation functional (B3LYP), with a basis set 6-31+G*, was used. The calculations were performed with the Gaussian03 (G03) [27] program. Time-Dependent Density Functional Theory (TD-DFT) [28,29] calculations provided the excitation energies of the ligands. The Conductor-like Polarizable Continuum Model (CPCM) [30-32], with chloroform as solvent, was used to calculate the electronic structure and the excited states of the ligands in solution. From the singlet ground state, optimized in the gas phase, 20 singlet excited states and corresponding oscillator strengths were determined. The TD-DFT calculation does not provide the electronic structure of the excited states; however, electronic distribution and localization of the singlet-excited states may be visualized using the Electron Density Difference Maps (EDDMs) [33]. GaussSum 3 [34] was used for EDDMs calculations and for the electronic spectrum simulation.

3. Results and discussion

3.1. ^1H and ^{13}C NMR spectra

Figures 1-4 depict the ^{1}H and ^{13}C NMR spectra for $\mathbf{L}^1$ and $\mathbf{L}^2$, respectively. In the ^{1}H NMR spectrum of the $\mathbf{L}^1$ ligand (Figure 1), the signals at $\delta = 12.87$ and $\delta = 12.82$ ppm are assigned to the $-$OH proton of carboxylic acid and the $-$OH proton of phenolic group, respectively. Furthermore, the azomethine proton is observed as a singlet at $\delta = 8.91$ ppm. The aromatic protons of the ligand appeared at $\delta = 6.80 - 7.95$ ppm. The H^e signal is observed at $\delta = 7.94$ ppm as a doublet, due to coupling with the H^d, and the H^d signal appears at $\delta = 7.41$ ppm as a doublet, due to its coupling with H^e. The H^c signal is observed at $\delta = 7.18$ ppm as a doublet, due to coupling with the H^b, and the H^a signal is observed at $\delta = 7.05$ ppm as a doublet, due to its coupling with the H^b. The H^b appeared at $\delta = 6.82$ ppm as a triplet, due to its coupling with H^a and H^c. A quartet at $\delta = 3.99$ ppm [^3J (H,H) = 7.0 Hz] is assigned to the $-$OCH$_2-$protons, coupled with the $-$CH$_3$ protons, while a triplet at $\delta = 1.27$ ppm [^3J (H,H) = 7.0 Hz] is assigned to the $-$CH$_3$ protons, coupled with the $-$OCH$_2$ protons. The ^{13}C NMR spectrum of ligand $\mathbf{L}^1$ (Figure 2) shows the two carboxylic and iminic carbons C(1) and C(6) resonances as functional group signals at 166.8 and 165.1 ppm, respectively. In the ^{1}H NMR spectrum of ligand $\mathbf{L}^2$ (Figure 3), a signal at $\delta = 12.97$ ppm is assignable to the $-$OH proton of carboxylic acid, while a signal at $\delta = 12.75$ ppm is assigned to the $-$OH phenolic proton. Furthermore, the azomethine proton is observed as a singlet at $\delta = 8.91$ ppm. The aromatic protons of the ligand appear at $\delta = 6.82 - 7.94$ ppm. The H^e signal is observed at $\delta = 7.93$ ppm as a doublet, due to coupling with the H$_d$, and the H^d signal appears at $\delta = 7.70$ ppm as a doublet, due to its couplings with H^d. The H^c signal is observed at $\delta = 7.19$ ppm as a doublet, due to coupling with the H^b, and the H^a signal is observed at $\delta = 7.07$ ppm as a doublet, due to coupling with the H^b. The H^b signal appears at $\delta = 6.84$ ppm as a triplet, due to its couplings with H^a and H^c. The ^{13}C NMR spectrum of the $\mathbf{L}^2$ ligand (Figure 4) shows the two carboxylic and iminic carbon, C(1) and C(8), resonances, as functional group signals at 166.8 and 164.9 ppm, respectively.

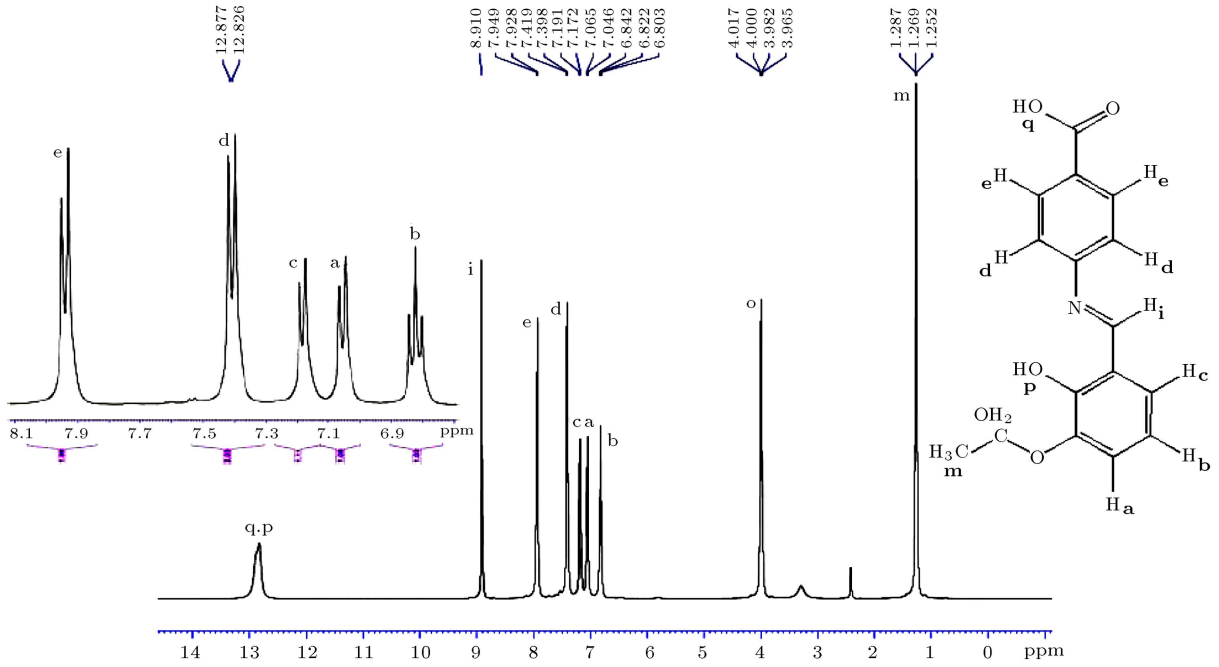

Figure 1. ^{1}HNMR spectrum of $\mathbf{L}^1$ with assignment of hydrogen atoms in the related scheme (the inset shows expansion).

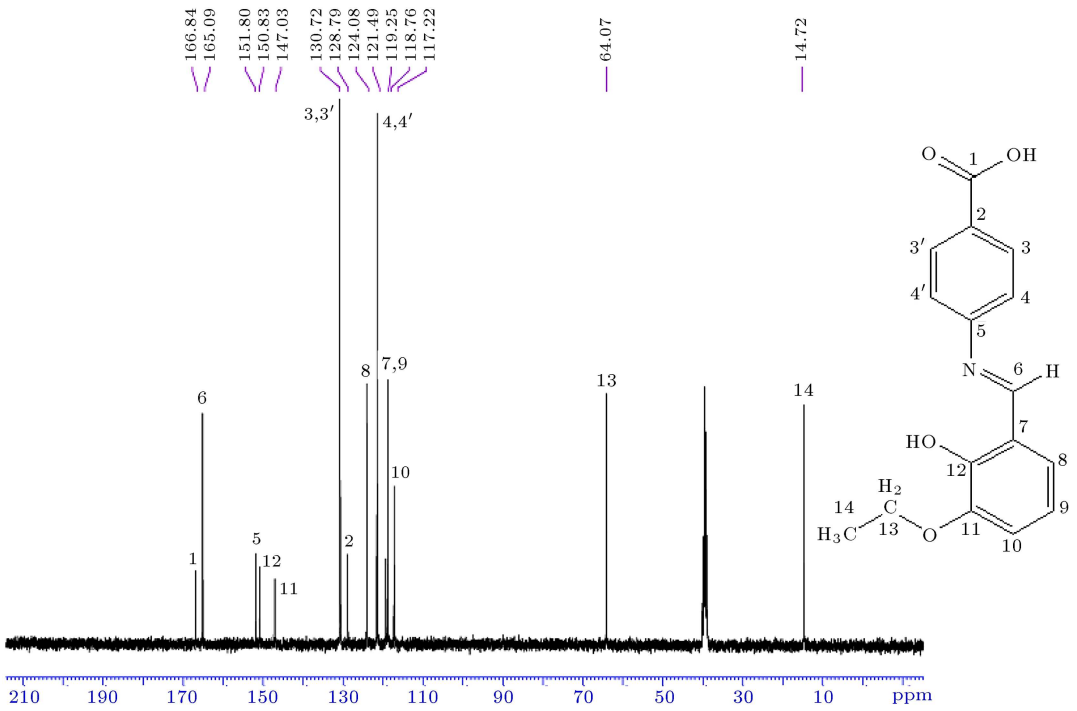

Figure 2. $^{13}C\{^{1}H\}$NMR spectrum of ligand $\mathbf{L}^1$.

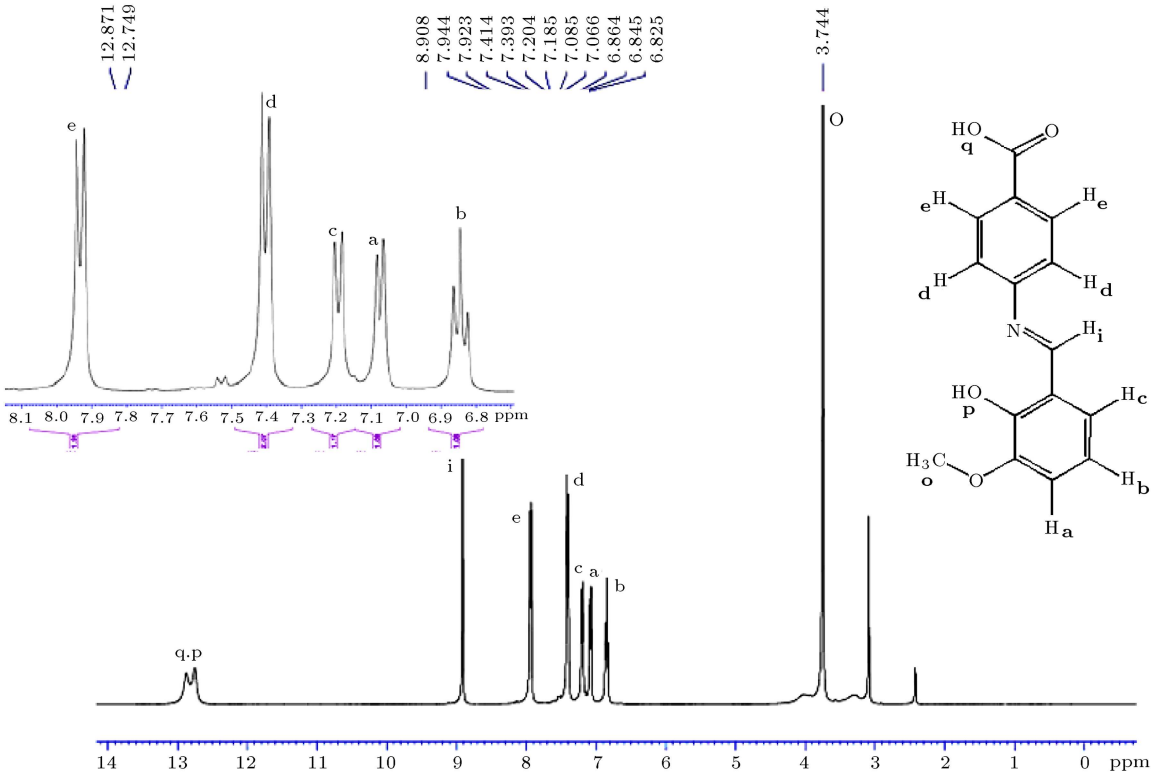

Figure 3. ^{1}HNMR spectrum of $\mathbf{L}^2$ with assignment of hydrogen atoms in the related scheme.

3.2. Electronic spectra

Figure 5 shows the overlay of UV-Vis spectra of $\mathbf{L}^1$ and $\mathbf{L}^2$. The electronic absorption spectra measured in a chloroform solution at room temperature show absorption bands, due to the transitions, $\pi \rightarrow \pi^*$, $n \rightarrow \pi^*$. The shoulders observed at 375 nm for $\mathbf{L}^1$ and $\mathbf{L}^2$ are attributed to the $\pi \rightarrow \pi^*$ transition of the substituted phenoxy ring to the imine and carboxyphenyl ring. The absorption bands at 318 and 320 nm for $\mathbf{L}^1$ and $\mathbf{L}^2$, respectively are due to $\pi \rightarrow \pi^*$ and $n \rightarrow \pi^*$ transitions

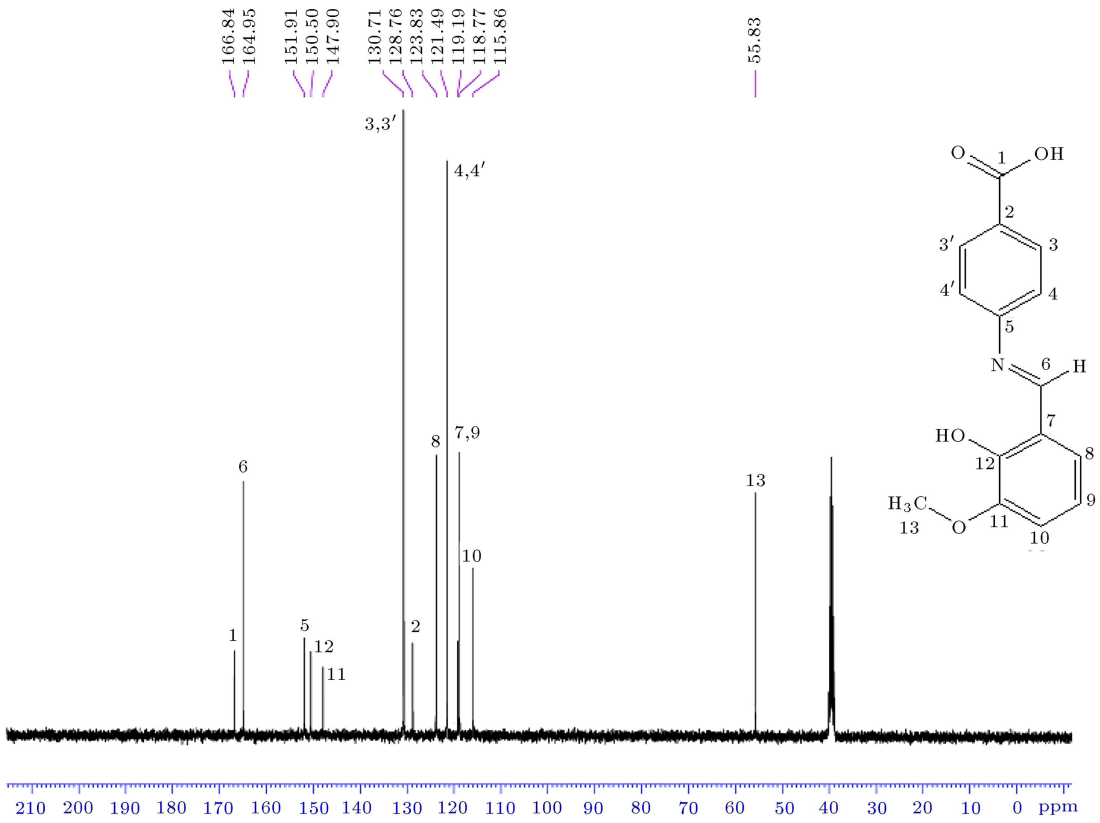

Figure 4. $^{13}C\{^1H\}$NMR spectrum of ligand $\mathbf{L}^2$.

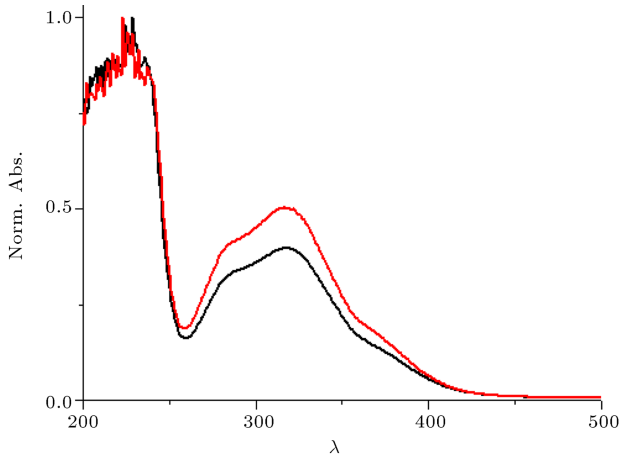

Figure 5. The UV-Vis spectra of $\mathbf{L}^1$ and $\mathbf{L}^2$ in $CHCl_3$.

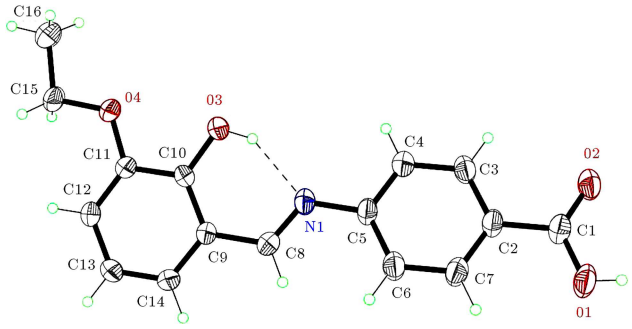

Figure 6. The molecular structure of $\mathbf{L}^1$, showing 40% probability displacement ellipsoids and the atomic numbering. The dashed lines show the intramolecular hydrogen bond.

of aromatic rings and imine segments. The bands at 225 and 227 nm are mainly due to the $\pi \rightarrow \pi^*$ transitions of aromatic rings.

3.3. FT-IR spectra

The most characteristic absorptions of the Schiff base ligands are summarized in the "Experimental" section. The $\nu_{asym}(-COO)$ and $\nu_{sym}(-COO)$ stretching vibrations are observed at 1425, 1423 and 1683, 1678 cm^{-1} for $\mathbf{L}^1$ and $\mathbf{L}^2$ ligands, respectively. The $\nu(C{=}N)$ bond of $\mathbf{L}^1$ and $\mathbf{L}^2$ ligands presents at 1591 and 1593 cm^{-1}, respectively.

3.4. Crystal structures of L^1 and L^2

Figures 6 and 7 depict the molecular structures of $\mathbf{L}^1$ and $\mathbf{L}^2$, respectively. Crystal data and refinement parameters are summarized in Table 1. Selected bond distances and bond angles are given in Table 2. The details of the hydrogen bonds are summarized in Table 3. Compound $\mathbf{L}^1$ crystallizes in the triclinic space group, $P-1$, with one molecule in the asymmetric unit. Compound $\mathbf{L}^1$ shows *trans* conformation around C8=N1 [1.275(2) Å] double bond, which is comparable to the bond length of the related Schiff bases [35,36]. The hydrogen atom of the hydroxyl group shows a strong intramolecular O–H···N hydro-

Table 1. Crystal data and refinement parameters for $\mathbf{L}^1$ and $\mathbf{L}^2$.

	$\mathbf{L^1}$	$\mathbf{L^2}$
Empirical formula	$C_{16}H_{15}NO_4$	$C_{15}H_{13}NO_4.CH_3OH$
Formula mass	285.29	303.31
Crystal size (mm)	$0.05 \times 0.10 \times 0.25$	$0.08 \times 0.12 \times 0.22$
Crystal system	triclinic	orthorhombic
Space group	P-1	$P2_12_12_1$
θ_{max} (°)	28.06	28.3
a (Å)	4.9897(3)	4.7824(4)
b (Å)	6.9109(5)	10.2031(11)
c (Å)	20.7694(15)	30.516(3)
α (°)	83.690(4)	90
β (°)	84.855(4)	90
γ (°)	78.698(4)	90
V (Å^3)	696.35(8)	1489.0(3)
Z	2	4
D_{calc} (Mg/m^3)	1.361	1.353
μ (mm^{-1})	0.099	0.101
$F(000)$	300	640
Index ranges	$-6 \le h \le 6$ $-9 \le k \le 9$ $-27 \le l \le 27$	$-5 \le h \le 6$ $-13 \le k \le 13$ $-40 \le l \le 40$
No. of measured reflections	11653	14540
No. of independent reflections/R_{int}	3337/0.047	3682/0.104
No. of observed reflections $I > 2\sigma(I)$	1712	1489
No. of parameters	193	206
Goodness-Of-Fit (GOF)	0.99	0.97
R_1 (observed data)	0.0523	0.0669
wR_2 (all data)[a]	0.1314	0.1822

[a]: $w = 1/[\sigma^2(F_o^2) + (0.0553P)^2]$ for $\mathbf{L}^1$,
$w = 1/[\sigma^2(F_o^2) + (0.0644P)^2]$ for $\mathbf{L}^2$ where $P = (F_o^2 + 2F_c^2)/3$

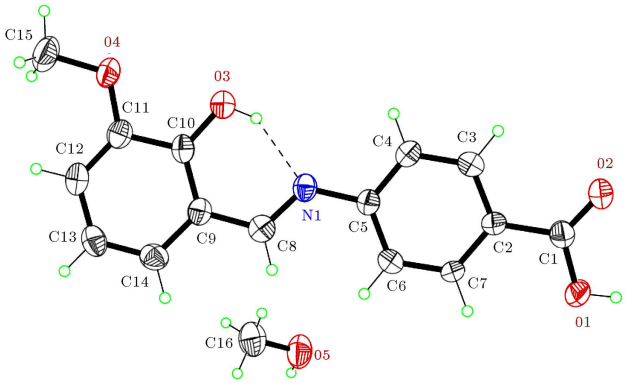

Figure 7. The molecular structure of $\mathbf{L}^2$ showing 40% probability displacement ellipsoids and the atomic numbering. The dashed lines show the intramolecular hydrogen bond.

Table 2. Selected bond lengths and angles of $\mathbf{L}^1$ and $\mathbf{L}^2$.

	$\mathbf{L^1}$	$\mathbf{L^2}$
C(8)-N(1)	1.275(2)	1.304(6)
C(8)-C(9)	1.445(2)	1.420(6)
C(10)-O(3)	1.344(2)	1.301(5)
C(1)-O(1)	1.272(2)	1.320(6)
C(1)-O(2)	1.259(2)	1.202(6)
O(3)-C(10)-C(9)	120.6(2)	122.9(4)
C(9)-C(8)-N(1)	122.2(2)	121.5(5)
C(8)-N(1)-C(5)	122.4(2)	123.8(4)
N(1)-C(5)-C(4)	116.2(2)	123.5(4)

gen bond. The dihedral angle between the C9-C14 and C2-C7 benzene rings is 20.47(9)°, which shows deviation from planarity. This deviation from planarity can be due to the significant intermolecular O–H$\cdots$O hydrogen bonds between the carboxylic groups and the intermolecular C–H$\cdots$p interaction by one of the hydrogen atoms of the ethoxy substituent [H15A], to the centroid of the aromatic ring [Cg (centroid of the ring) =C9/C10/C11/C12/C13/C14] of the neighboring molecule [C15$\cdots$Cg = 3.580(2) Å, C15–H15A$\cdots$Cg = 148°)]. In the crystal packing of $\mathbf{L}^1$, molecules are connected together by pairs of centerosymmetric intermolecular O–H$\cdots$O hydrogen bonds of the carboxylic

Table 3. Parameters of hydrogen bonding in $\mathbf{L}^1$ and $\mathbf{L}^2$.

	D-H···A	H···A (Å)	D···A (Å)	D-H···A (°)
$\mathbf{L^1}$	O1-H1···O2$^{(i)}$	1.82	2.624(2)	168
	O3-H3A···N1	1.86	2.589(2)	147
$\mathbf{L^2}$	O1-H1···O5$^{(ii)}$	1.83	2.633(6)	165
	O3-H3A···N1	1.85	2.560(5)	144
	O5-H5···O3$^{(iii)}$	1.99	2.773(5)	157
	C8-H8···O2$^{(iv)}$	2.55	3.418(6)	155

Symmetry codes: $^{(i)}$: $3-x, 1-y, -z$; $^{(ii)}$: $2-x, 1/2+y, 1/2-z$; $^{(iii)}$: $1+x, -1+y, z$; and $^{(iv)}$: $1-x, -1/2+y, 1/2-z$.

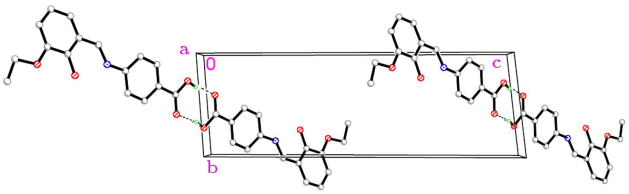

Figure 8. The crystal packing of $\mathbf{L}^1$ viewed down the a-axis showing individual dimer formation by pairs of centerosymmetric O-H···O hydrogen bonds.

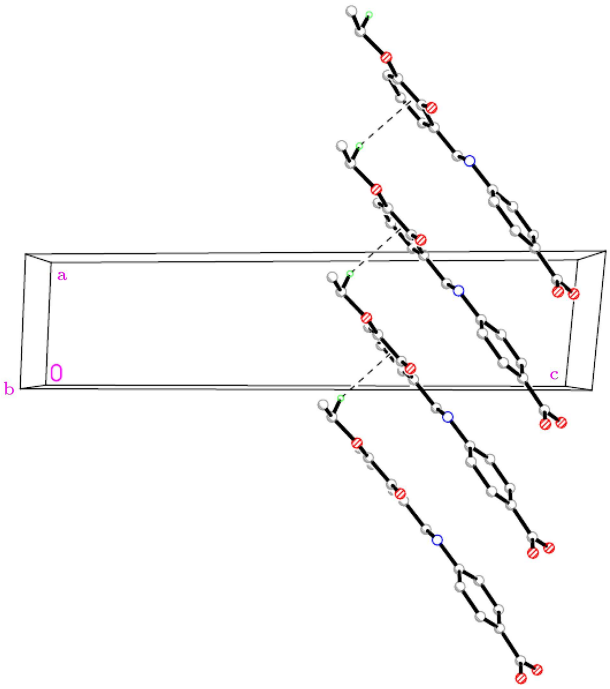

Figure 9. The crystal packing of $\mathbf{L}^1$ viewed down the a-axis showing column of molecules connected by C-H···π interaction.

groups, forming individual dimers (Figure 8). The crystal packing, depicting the intermolecular C-H...π interaction of L_1, is shown in Figure 9. Compound $\mathbf{L}_2$ crystallizes in the orthorhombic chiral space group, $P2_12_12_1$, with one molecule in the asymmetric unit and a methanol solvent of crystallization. Similar to $\mathbf{L}_1$, compound $\mathbf{L}_2$ also shows trans conformation around C8=N1 [1.304(6)Å] double bond. In the case of $\mathbf{L}_2$, the

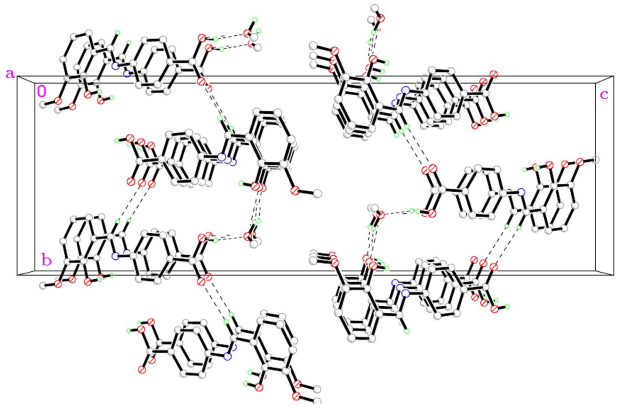

Figure 10. The crystal packing of $\mathbf{L}^2$ viewed down the a-axis showing connection of molecules into infinite one-dimensional chain along the b-axis.

dihedral angle between the C9-C14 and C2-C7 benzene rings is 6.4(2)Å, which shows almost planarity. Also, in this case, there are no O−H...O hydrogen bonds between the carboxylic groups and significant intermolecular C−H...π interactions. The crystal packing of $\mathbf{L}_2$ shows intermolecular O−H:.O hydrogen bonds between the methanol solvent of crystallization, O−H groups of the phenolic and carboxylic segments and C−H...O interactions between iminic hydrogen and oxygen atom of the carboxylic group, which form chain of molecules along the b-axis of the unit cell (Figure 10). Regarding the chiral space group of $\mathbf{L}_2$, the Flack parameter [37] could not be determined in the absence of sufficient anomalous scattering.

3.5. Computational details

Selected important frontier molecular orbitals for $\mathbf{L}^1$ and $\mathbf{L}^2$ are depicted in Figure 11. Data for the composition of the most important occupied and virtual orbitals, and the atomic orbital contributions for each ligand (%) are listed in Table 4. In the frontier region, neighboring orbitals are often closely spaced. In such cases, consideration of only the HOMO and LUMO may not yield a realistic description. For this reason, Density Of State (DOS) diagrams, which incorporate a degree of overlap between the curves convoluted from neighboring energy levels, can give a

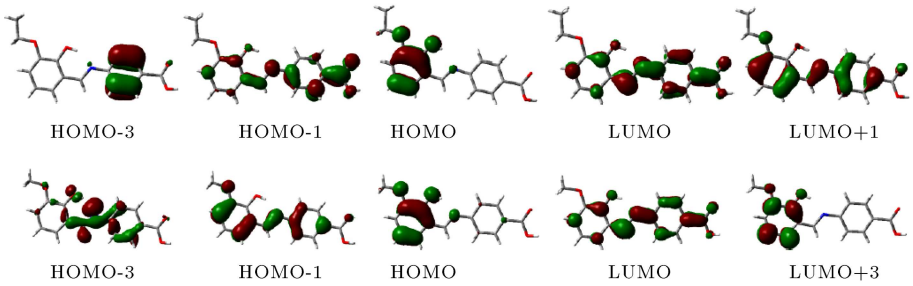

Figure 11. Selected frontier molecular orbitals of $\mathbf{L}^1$ and $\mathbf{L}^2$.

Table 4. G03/B3LYP calculated one-electron energy and percentage composition of selected frontier MOs of $\mathbf{L}^1$ and $\mathbf{L}^2$ expressed in terms of component fragments.

	MO	Energy (eV)	Character	−PhCOOH (1)	−Imine (2)	−PhOEt (3)
$\mathbf{L}^1$	79(V)	-0.04	1	91	1	8
	78(V)	-0.68	3	7	1	92
	77(V)	-1.03	3	7	3	90
	76(V)	**-2.28**	**1+2+3**	**43**	**32**	**25**
	75(O)	**-7.83**	**3**	**2**	**2**	**96**
	74(O)	-6.00	1+3	38	13	49
	73(O)	-6.52	1+2+3	35	34	31
	72(O)	-7.36	1	100	0	0
	MO	**Energy (eV)**	**Character**	**−PhCOOH (1)**	**−Imine (2)**	**−PhOEt (3)**
$\mathbf{L}^2$	75(V)	-0.09	3	1	5	94
	74(V)	-0.63	1	93	0	7
	73(V)	-0.93	1	68	14	18
	72(V)	**-2.34**	**1+2+3**	**40**	**34**	**26**
	71(O)	**-5.94**	**3**	**5**	**4**	**91**
	70(O)	-6.45	1+3	30	14	56
	69(O)	-7.41	1	92	5	3
	68(O)	-7.46	1+2	29	55	16

Energy gap (ΔE) = 5.5 and **3.60 eV** (HOMO-LUMO), for **1** and **2**, respectively.

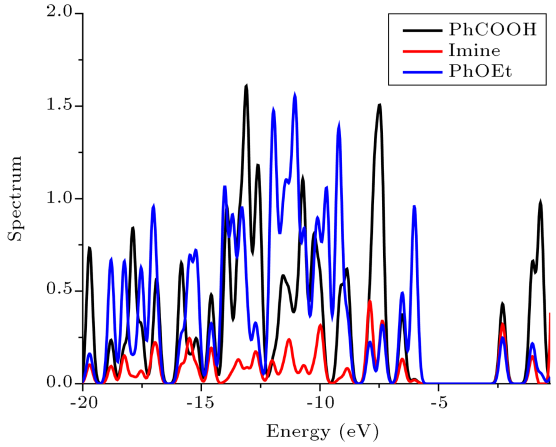

Figure 12. The DOS spectrum of $\mathbf{L}^1$ with the contribution of different segments.

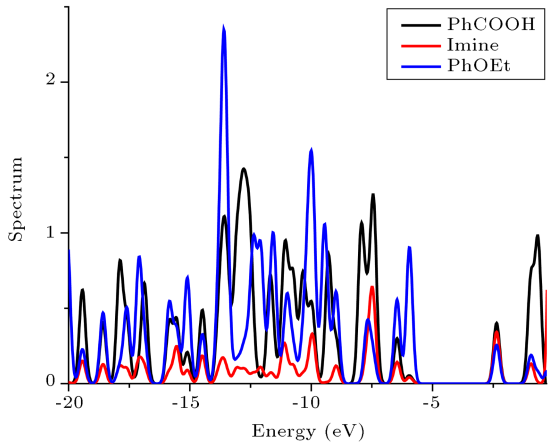

Figure 13. The DOS spectrum of $\mathbf{L}^2$ with the contribution of different segments.

more representative picture. The density of state of $\mathbf{L}^1$ and $\mathbf{L}^2$, plotted as a function of orbital energy (eV), are shown in Figures 12 and 13. Each ligand is divided into three parts: for $\mathbf{L}^1$: 1) the PhCOOH (phenylcarboxylic segment, 1), 2) the imine group (segment 2), and 3) the -PhOEt (o-ethoxy-hyroxyphenyl segment 3) and for $\mathbf{L}^2$, 1) the PhCOOH (phenylcarboxylic segment, 2) the imine group (segment 2) and 3) PhOMe (o-methoxyhyroxyphenyl segment 3). Each part of the percentage contributions are the sum of the atomic

orbital coefficient squares. As shown in Figure 11, the highest occupied orbitals (HOMO) in both ligands have a predominant segment 1 (−PhOEt in $\mathbf{L}^1$ and −PhOMe in $\mathbf{L}^2$) character, i.e. 96 and 90%, respectively. The LUMO orbitals are primarily localized on all three segments with 43, 32, and 25% for $\mathbf{L}^1$, and 40, 24, 36% for $\mathbf{L}^2$. Some higher-energy occupied MOs (LUMO + 1 and LUMO + 2 in $\mathbf{L}^1$) have the predominant character of segment 3 (−PhOEt), but, for $\mathbf{L}^2$, these orbital have the predominant character of segment 1 (−PhCOOH).

The simulated optical absorption spectra of $\mathbf{L}^1$ and $\mathbf{L}^2$ shown in Figure 14, reproduce the main features

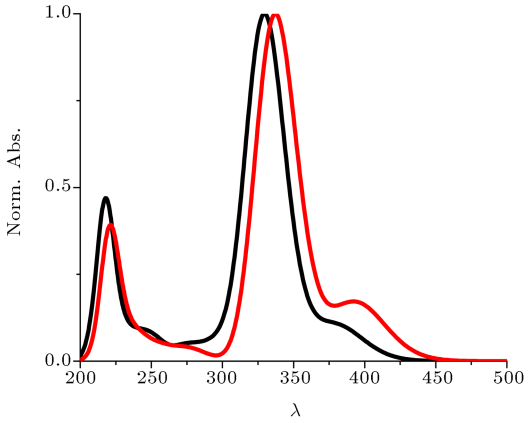

Figure 14. The simulated UV-Vis spectra of $\mathbf{L}^1$ (black) and $\mathbf{L}^2$ (red).

of the experimental spectrum. TD-DFT computations were performed to predict the electronic transition energies and intensities of the 20 lowest energy singlet transitions of the ligands. Selected low-lying singlet excited states, together with their oscillator strengths and assignment for $\mathbf{L}^1$ and $\mathbf{L}^2$, are displayed in Table 5. Electron Density Difference Maps (EDDMs) derived from the TD-DFT calculations were used to show the electron density changes between the ground and excited states, upon different electronic excitations (Figure 15). It represents a way for visualizing electronic distribution for which one can subtract the ground-state electron density (S_0) from the Franck-Condon electron density of the excited state, thereby, providing a picture of the redistribution of the electron density after the vertical transition from the ground-state to any of the Franck-Condon excited states. Visualization of these difference density plots allows the changes to the electronic features on the excited-state surface to be more easily determined. They can provide an insight into the subsequent geometric changes occurring on the excited-state potential energy surface [38], and determine what type of excitation is occurring. As expected, the lower energy bands (the shoulder in 379 and 329 nm for $\mathbf{L}^1$ and 393 and 336 for $\mathbf{L}^2$) in the spectrum arise from transitions that are mainly $\pi \rightarrow \pi^*$ and $n \rightarrow \pi^*$ of the substituted phenoxy ring to the imine and carboxyphenyl ring and aromatic rings and imine segment, respectively. The higher-energy bands

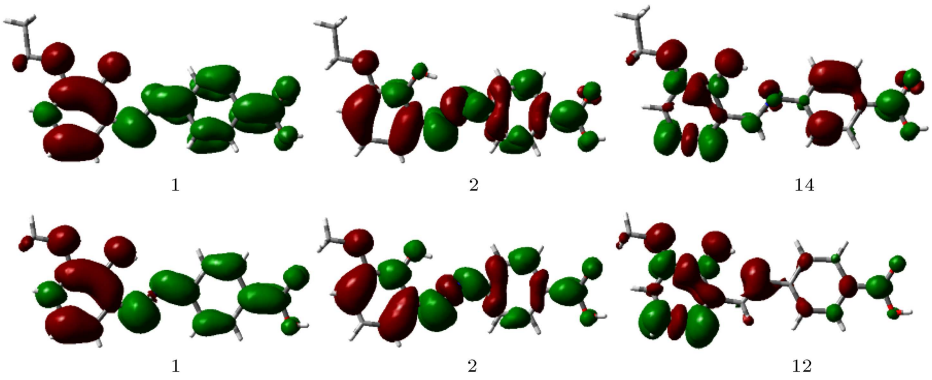

Figure 15. Electron Density Difference Maps (EDDMs) for main transitions 1, 2, and 14 for $\mathbf{L}^1$, and 1, 2, and 12 for $\mathbf{L}^2$. Red indicates a decrease in charge transfer, while green indicates an increase.

Table 5. Selected TD-DFT calculated excitation energies and compositions of the lowest lying singlet excited states for $\mathbf{L}^1$ and $\mathbf{L}^2$.

	States	E(eV)/λ(nm)	f	λ_{exp}	Transition	Assignment
$\mathbf{L}^1$	1	3.26/379	0.104	375	$\mathbf{H} \rightarrow \mathbf{L}$ (92%)	$\pi \rightarrow \pi^*$
	2	3.76/329	1.01	318	$\mathbf{H}-1 \rightarrow \mathbf{L}$ (85%)	$\pi \rightarrow \pi^*$, $n \rightarrow \pi^*$
	14	5.71/217	0.217	225	$\mathbf{H}-3 \rightarrow \mathbf{L}+1$ (21%), $\mathbf{H} \rightarrow \mathbf{L}+3$ (46%)	$\pi \rightarrow \pi^*$
$\mathbf{L}^2$	1	3.15/393	0.174	375	$\mathbf{H} \rightarrow \mathbf{L}$ (90%)	$\pi \rightarrow \pi^*$
	2	3.68/336	1.03	320	$\mathbf{H}-1 \rightarrow \mathbf{L}$ (87%)	$\pi \rightarrow \pi^*$, $n \rightarrow \pi^*$
	12	5.58/222	0.256	227	$\mathbf{H} \rightarrow \mathbf{L}+3$ (60%)	$\pi \rightarrow \pi^*$

H and **L** refer to the highest-occupied and lowest-unoccupied molecular orbitals, respectively.

are also due to the $\pi \rightarrow \pi^*$ transitions of aromatic rings.

4. Conclusion

Two new 4-aminobezoic acid derived Schiff base ligands were synthesized by the condensation reaction of 3-ethoxy and 3-methoxysalicyaldehyde with 4-aminobenzoic acid, and characterized by spectroscopic methods and X-ray diffraction analysis. The ground and excited states of the new compounds were studied by DFT and TD-DFT methods.

5. Supplementary materials

Crystallographic data (excluding structure factors) for the structural analysis have been deposited with the Cambridge Crystallographic Data Centre, CCDC Nos. 895770 ($\mathbf{L}^1$) and 895771 ($\mathbf{L}^2$). Copies of this information may be obtained free of charge via http://www.ccdc.cam.ac.uk/conts/retrieving.html or from The Director, CCDC, 12 Union Road, Cambridge, CB2 1EZ, UK (fax: + 44-1223-336-033; e-mail: deposit@ccdc.ac.uk). The ^{13}CNMR of $\mathbf{L}^1$ and $\mathbf{L}^2$ are included in the supplementary materials.

Acknowledgments

RK thanks Sharif University of Technology Research Council for use of their facilities, and HK thanks Payame Noor University for financial support of this work.

References

1. Holm, R.H., Everett, G.W. and Chakravorty, A., *Progress in Inorganic Chemistry*, John Wiley & Sons, INC: New York, London, Sydney, **7**, pp. 83-113 (1966).
2. Chohan, Z.H., Arif, M., Shafiq, Z., Yaqub, M. and Supuran, C.T. "In vitro antibacterial, antifungal & cytotoxic activity of some isonicotinoylhydrazide Schiff's bases and their cobalt (II), copper (II), nickel (II) and zinc (II) complexes", *J. Enzyme Inhib. Med. Chem.*, **21**, pp. 95-103 (2006).
3. Ren, S., Wang, R., Komatsu, K., Bonaz-Krause, P., Zyrianov, Y., McKenna, C.E., Csipke, C., Tokes, Z.A. and Lien, E.J. "Synthesis, biological evaluation, and quantitative structure-activity relationship analysis of new Schiff bases of hydroxysemicarbazide as potential antitumor agents", *J. Med. Chem.*, **45**, pp. 410-419 (2002).
4. Hodnett, E.M. and Dunn, W.J. "Structure-antitumor activity correlation of some Schiff bases", *J. Med. Chem.*, **13**, pp. 768-770 (1970).
5. Dhar, D.N. and Taploo, C.L. "Schiff bases and their applications", *J. Sci. Ind. Res.*, **41**, pp. 501-506 (1982).
6. Dey, K.J. "Schiff bases and their applications", *Sci. Ind. Res.*, **33**, pp. 76-97 (1974).
7. Kumar, S., Dhar, D.N. and Saxena, P.N. "Schiff bases and their applications", *J. Sci. Ind. Res.*, **41**, pp. 501-506 (1980).
8. Deshmukh, M.D. and Doshi, A.G. "Synthesis of Schiff bases and their applications", *Orient. J. Chem.*, **11**, pp. 86-96 (1995).
9. Armistead, W.H. and Stookey, S.D. "Photochromic silicate glasses sensitized by silver halides", *Science*, **144**, pp. 150-154 (1964).
10. Sousa, J.A. and Kashnow, R.A. "Photochromic paper for imaging ultraviolet laser pulses", *Rev. Sci. Instrum.*, **40**, pp. 966-967 (1969).
11. Harada, J., Uekusa, H. and Ohashi, Y. "X-ray analysis of structural changes in photochromic salicylideneaniline crystals. Solid-state reaction induced by two-photon excitation", *J. Am. Chem. Soc.*, **121**, pp. 5809-5810 (1999).
12. Kawata, S. and Kawata, Y. "Three-dimensional optical data storage using photochromic materials", *Chem. Rev.*, **100**, pp. 1777-1788 (2000).
13. Kohei, J., Takashi, I., Akiko, Se., Hidehiro, U. and Yuji, O. "Relation between photochromic properties and molecular structures in salicylideneaniline crystals", *Acta Cryst*, **B68**, pp. 297-304 (2012).
14. Cohen, M.D. and Schmidt, G.M. "Photochromy and thermochromy of anils", *J. Chem. Phys.*, **66**, pp. 2442-2447 (1962).
15. Nazeeruddin, M.K. and Graetzel, M. "Transition metal complexes for photovoltaic and light emitting applications", *Struct. Bonding*, **123**, pp. 113-175 (2007).
16. Graetzel, M. "Solar energy conversion by dye-sensitized photovoltaic cells", *Inorg. Chem.*, **44**, pp. 6841-6851 (2005).
17. Polo, A.S., Itokazu, M.K. and Iha, N.Y.M. "Metal complex sensitizers in dye-sensitized solar cells", *Coord. Chem. Rev.*, **248**, pp. 1343-1361 (2004).
18. Ardo, S. and Meyer, G.J. "Photodriven heterogeneous charge transfer with transition-metal compounds anchored to TiO_2 semiconductor surfaces", *Chem. Soc. Rev.*, **38**, pp. 115-146 (2009).
19. Constable, E.C., Hernandez, A.R., Housecroft, C.E., Neuburger, M. and Schaffner, S. "Copper(I) complexes of 6,6′-disubstituted 2,2′-bipyridine dicarboxylic acids: new complexes for incorporation into copper-based dye sensitized solar cells (DSCs)", *Dalton Trans.*, pp. 6634-6644 (2009).
20. Constable, E.C., Housecroft, C.E., Neuburger, M., Price, J., Wolf, A. and Zampese, J.A. "A strategy for controlling charge and conformation in 2,2′-bipyridine complexes for use in photonic applications", *Inorg. Chem. Commun.*, **13**, pp. 74-76 (2010).
21. SMART, Bruker Molecular Analysis Research Tool, Bruker AXS Inc., Madison, Wisconsin, USA (2005).

22. SAINT (Version V7.12A), Data Reduction and Correction Program, Bruker AXS Inc., Madison, Wisconsin, USA (2005).

23. SADABS (Version 2004/1). An Emprical Absorption Correction Program. Bruker AXS Inc., Madison, Wisconsin, USA (2004).

24. Sheldrick, G.M. "A history of SHELXL", *Acta Cryst. Sect*, **A64**, pp. 112-122 (2008).

25. Becke, A.D. "Density-functional thermochemistry. III. The role of exact exchange", *J. Chem. Phys.*, **98**, pp. 5648-5652 (1993).

26. Lee, C., Yang, W. and Parr, R.G. "Development of the Colle-Salvetti correlation-energy formula into a functional of the electron density", *Phys. Rev. B: Condens Matter*, **37**, pp. 785-789 (1998).

27. Frisch, M.J. et al. *Gaussian 03*, Revision **B.04**, Gaussian, Inc.: Wallingford, CT (2004).

28. Stratmann, R.E., Scuseria, G.E. and Frisch, M.J. "An efficient implementation of time-dependent density-functional theory for the calculation of excitation energies of large molecules", *J. Chem. Phys.*, **109**, pp. 8218-8224 (1998).

29. Casida, M.E., Jamorski, C., Casida, K.C. and Salahub, D.R. "Molecular excitation energies to high-lying bound states from time-dependent density-functional response theory: Characterization and correction of the time-dependent local density approximation ionisation threshold", *J. Chem. Phys.*, **108**, pp. 4439-4449 (1998).

30. Barone, V. and Cossi, M. "Quantum calculation of molecular energies and energy gradients in solution by a conductor solvent model", *J. Phys. Chem.*, **A102**, pp. 1995-2001 (1998).

31. Cossi, M. and Barone, V. "Time-dependent density functional theory for molecules in liquid solutions", *J. Chem. Phys.*, **115**, pp. 4708-4717 (2001).

32. Cossi, M., Rega, N., Scalmani, G. and Barone, V. "Energies, structures, and electronic properties of molecules in solution with the C-PCM solvation model", *J. Comput. Chem.*, **24**, pp. 669-681 (2003).

33. Browne, W.R., O'Boyle, N.M., McGarvey, J.J. and Vos, J.G. "Elucidating excited state electronic structure and intercomponent interactions in multicomponent and supramolecular systems", *Chem. Soc. Rev.*, **34**, pp. 641-663 (2005).

34. O'Boyle, N.M. and Vos, J.G. "cclib: A library for package-independent computational chemistry algorithms", *GaussSum 3, J. Comp. Chem.*, **29**, pp. 839-845 (2008).

35. Alizadeh, K. and Morsali, A. "Crystal structure of pyridinyl-2-methylene-4-aminobenzoic acid", *Anal. Sci.*, **27**, pp. 11-12 (2011).

36. Jiang, C.F., Liang, F.P., Li, Y., Wang, X.U., Chen, Z.L. and Bian, H.D. "Synthesis, characterization and magnetic properties of copper(II) complexes with 4-N-(2′-pyridylimine)benzoic acid", *J. Mol. Struct.*, **842**, pp. 109-116 (2007).

37. Flack, H.D. "On enantiomorph-polarity estimation", *Acta. Cryst. Sec*, **A39**, pp. 876-888 (1984).

38. Wiberg, K.B., Hadad, C.M., Breneman, C.M., Laidig, K.E., Murcko, M.A. and LePage, T.J. "The eesponse of electrons to structural changes", *Science*, **252**, pp. 1266-1272 (1991).

Biographies

Reza Kia was born in 1975. He obtained his MS and PhD degrees in Inorganic Chemistry, respectively, from Shiraz University, in 2001, and University of Isfahan, Iran, in 2005. He has held postdoctoral positions at the University of Bath, UK, University Sains Malaysia, the Max Planck Institute for Biophysical Chemistry (MPI) in Goettingen, and the Deutsches Elektronen-Synchrotron (DESY) in Hamburg, Germany. He is currently Assistant Professor of Inorganic Chemistry in the Chemistry Department of Sharif University of Technology, Tehran, Iran. His research interests include laboratory and synchrotron-based Chemical Crystallography and Photocrystallography, and Structural Inorganic Chemistry.

Hadi Kargar was born in 1977. He obtained his BS, MS and PhD degrees from the University of Isfahan, Iran, and is currently Associate Professor of Inorganic Chemistry in Payame Noor University of Ardakan. His research interests include synthesis, characterization and catalytic properties of coordination complexes, with focus on Schiff bases complexes and metalloporphyrins.